

Tropical Skin Disease Classification using Connected Attribute Filters

Fred N. Kiwanuka¹, Omar Eltaher Abuelmaatti¹, Anang Hudaya Muhamad Amin¹
and Brian J. Mukwaya²

¹*Division of Computer and Information Science, Higher Colleges of Technology, Dubai, U.A.E.*

²*PredictX, Uganda*

Keywords: Max Tree, Connected Operators, Connected Filters, Attribute Filters, Skin Diseases, Deep Learning.

Abstract: Morphological connected filters operate on an image through flat zones which comprise the largest connected components with a constant signal. These filters identify and ultimately extract the whole connected components in an image without alteration of their boundaries and thus shape preserving. This is a desirable property in many image processing and analysis applications. However, due to the variability of the number of connected components, even in the case of images of the same resolution and size, their application in classification tasks has been limited. In this study, we propose an approach that computes the shape and size features of connected components and use these features for the classification of bacterial and viral tropical skin infections. We demonstrate the performance of the approach using gradient boosting machines and compare the results to deep learning approaches. Results show that the performance of our approach is comparable to that of Convolutional Neural Networks (CNN) based approach when trained on 1460 images. Moreover, CNN was pre-trained and required augmentation to achieve that performance. However, our approach is at least 56% faster than CNN.

1 INTRODUCTION

Mathematical morphology has contributed a wide range of operators to image processing and analysis. A number of efficient algorithms have been developed for image representation and description. These operators (Salember and Serra, 1995; Heijmans, 1999) have been used in many applications including; medical image processing (Kiwanuka et al., 2009a), image segmentation and reconstruction (Salember, 2015), object detection and recognition (Urbach, 2015), document analysis (Ouzounis and Wilkinson, 2011), characters recognition (Mennillo et al., 2015) video processing (Salember et al., 1998), color processing (van de Gronde and Roerdink, 2014) as well as remote sensing (Soille, 2008).

For many of these applications, an important task is to extract particular regions of an image while preserving as much of the contour information as possible. This is what has made connected filters (Salember and Wilkinson, 2009), a strictly edge preserving class of operators in mathematical morphology, a popular choice of selection. These operators act by merging flat zones, given some criteria, and filter an image without introducing new contours. They operate on connected components rather than pixels.

A sub-class of connected filters are attribute filters (Breen and Jones, 1996; Salember et al., 1998). They allow filtering based on the properties or *features* of connected components in the image. Examples of attribute filters include attribute openings, closings, thickenings, and thinnings (Meijster and Wilkinson, 2002; Breen and Jones, 1996; Salember et al., 1998) (Urbach et al., 2007; Westenberg et al., 2007). Attribute openings (Breen and Jones, 1996; Salember et al., 1998) allow the use of size based features. By contrast, attribute thinnings allow the use of shape-based features, which require translation, scale and rotation of invariant descriptors.

Although connected filters have been popular in many image processing and analysis tasks, they have hardly been used in classification tasks. This is because the majority of image classification tasks require all images to be of a fixed size. However the number of connected components in images of even the same pixel size varies depending on a number of factors including connectivity of the pixels. Connected and attribute filters extract connected components using the notion of connectivity. Connectivity describes the way pixels are grouped to form connected components or flat zones in a grayscale image. An example is shown in figure 1. As can be seen in

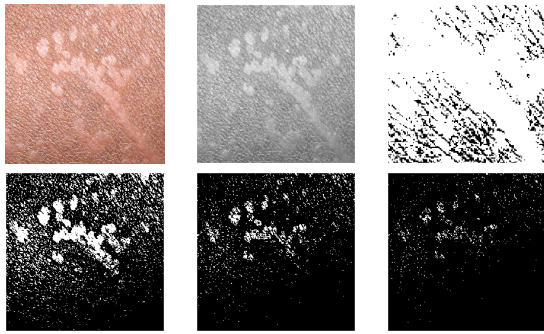


Figure 1: Sample viral infection image (left) with its grayscale and connected peak components representation at different threshold levels.

figure 1, the image contains object like patches and hence makes conclusive sense to engineer features with the notion of objects. In this paper, we propose a classification approach based on the features of connected components rather than pixels. We use images of skin infection to demonstrate our idea.

Skin diseases classification has proven to be challenging for many approaches in the literature, including deep learning due to diversity due to color, exposure, scale, level of details, illumination and appearance.

The paper is organized as follows. A brief background of the skin disease classification challenge is first presented in Section 2. In Section 3, the theory of connected and attribute filters is described; while data collection is covered in Section 4. Feature engineering is covered in Section 5. This includes the attributes description, and the Max-Tree approach. In Section 6, the performance evaluation of our approach is presented including a discussion of the results. We give concluding remarks in Section 7.

2 SKIN DISEASES IN TROPICAL REGIONS

According to a global dermatology report published in 2017 (Karimkhani et al., 2017), skin diseases represent up to 23.7% of the main organ-specific reasons for visiting a primary healthcare centre in Sub Sahara Africa. In Uganda, the cause of death attributed to skin diseases in 2017 was 0.36% of total deaths. The cause of a skin infection depends on the type of infection. The most common skin conditions in Sub Sahara Africa are attributed to bacterial, viral and fungal infections. According to the World health Organization, this is attributed mainly to the hot humid climates, poor living conditions and overcrowding.

Bacterial skin infections often begin as small, red bumps that slowly increase in size. Some bacterial infections are mild and easily treated with topical antibiotics, however other infections require an oral antibiotic. There are different types of bacterial skin infections including; cellulitis, impetigo, boils, and leprosy.

Viral skin infections are caused by a virus. These infections range from mild to severe. Examples of viral infections include; shingles (herpes zoster), chickenpox, Molluscum contagiosum, warts, measles, and hand, foot, and mouth disease.

Fungal skin infections are caused by a fungus and are most likely to develop in damp areas of the body, such as the feet or armpit. Many fungal infections are typically non-life-threatening and can include athlete's foot, yeast infection, ringworm, nail fungus, oral thrush, and diaper rash.

A variety of skin tests may be performed to diagnose skin allergies, bacterial, viral, or fungal skin infections. A culture test is a widely used method that is done to identify the microorganism (bacteria, fungus, or virus) that cause the infection. Skin (surface scrapings, biopsies, contents of pus bumps and blisters), hair, or nails may be cultured to detect bacteria, fungi, or viruses. However, poverty and a very high patients-to-dermatologist ratio in Sub Saharan African countries hinders proper diagnosis using culture tests. The commonest diagnosis in these countries is often, visual inspection of symptoms based on the appearance and location. This leads to misdiagnosis and unnecessary economic burden since some infections do not require medication. For example some types of viral skin infections may improve on their own and heal within days or weeks.

The boundary between these two cases in many diagnoses is difficult to be drawn. To illustrate the nature of this problem, and its difficulties, we show examples of image patches as shown in Fig. 2. In this research we attempt to automate this boundary separation using machine learning. We focus on viral and bacterial as there was no sufficient data for fungal infection.

2.1 Related Work

A number of studies have looked at image processing and computer vision methodology for automated diagnosis of skin diseases. (Liao et al., 2018), investigated the feasibility of constructing a universal skin disease diagnosis system using deep Convolutional Neural Networks (CNN). They trained the CNN architecture using 23,000 skin disease images from the Dermnet dataset and tested its performance on



Figure 2: Sample images, viral images at the top and bacterial cases at the bottom.

Dermnet and OLE skin disease open dataset. Another study by (Sun et al., 2016), introduced a benchmark multiclass dataset for clinical skin diseases for classification. They used 6,584 images from 198 classes of varying scale, some color, shape and structure and used CNN for the classification. A number of other studies have proposed other approaches for a review see (Barati et al., 2011), (Bi et al., 2017), (Romero-Lopez et al., 2017), (Pomponiu et al., 2016).

Unlike these approaches, our approach is connected component based rather than pixel based. They also utilized open sourced popular datasets of dermoscopic images, none of which is from tropical region based that comes with its own challenges of disease.

In this research we use real field conditions of skin infection datasets taken using a mobile phone in Uganda and to the best of our knowledge connected filters have not been used in classification tasks of this nature. An attempt to use them was made in (Quinn et al., 2014).

3 CONNECTED FILTERS

This section briefly reviews the concept of connected attribute filters. Let binary images X, Y be subsets of E , where E is a non-empty universal set with $\mathcal{P}(E)$ being a family of all subsets of E . If the images are grey-scale then it becomes a mapping from E to some subset of \mathbb{R} or \mathbb{Z} . We say a set $C \subseteq X$ is a *connected component* of X if C is connected, and if there is any other such that *connected set* D , $C \subseteq D \subseteq X$ then C is equal to D (Kiwanuka and Wilkinson, 2015).

3.1 Attribute Filters

An operator ψ (Heijmans, 1999) operating on binary image X is connected if and only if the set difference $X \setminus \psi(X)$ is exclusively composed of the connected

components of X or its complement X^c . To extract connected components from images, we use a family of operators called *connectivity openings*. Let $\Gamma_x(X)$ be the connectivity openings $x \in E$, $\Gamma_x(X)$ returns all the connected sets within X that have a point $x \in E$ in their intersection. If the union is C , then $C \subseteq X$, such that $x \in C$, is the maximal connected set containing x (Serra, 1998).

Given $\Gamma_x(X)$ of X at a point $x \in E$ with C a subset of $\mathcal{P}(E)$, binary connectivity opening are defined in (Kiwanuka and Wilkinson, 2015) as :

$$\Gamma_x(X) = \begin{cases} \bigcup \{C_i \in \mathcal{C} | x \in C_i, C_i \subseteq X\} & \text{if } x \in X \\ \emptyset & \text{otherwise.} \end{cases} \quad (1)$$

$\mathcal{C} \subseteq \mathcal{P}(E)$ is the family of all connected sets in E . A class of connectivity openings has the properties of: (i) *anti-extensive* since $\Gamma_x(X) \subseteq X$, (ii) *increasing* since $X \subseteq Y \Rightarrow \Gamma_x(X) \subseteq \Gamma_x(Y)$ this is the case of size based filtering criteria. It becomes non-increasing for shape based and (iii) *idempotent* since $\Gamma_x(\Gamma_x(X)) = \Gamma_x(X)$.

Once the connected components have been extracted, then attributes to filter the connected components is then computed. This where *attribute filters* (Breen and Jones, 1996; Salembier et al., 1998), a family of connectivity openings that imposes constraints on the connected components they return comes in. The constraints are expressed in the form of a binary criteria to make a decision of whether to accept or to reject components. Breen and Jones (Breen and Jones, 1996) define the attribute criterion as:

$$\Lambda(C) \equiv Attribute(C) \geq \lambda, \quad (2)$$

with $Attribute(C)$ is the attribute of the connected component C and λ the threshold. In our classification task, our interest is this attribute computed here.

After extracting the connected components using connectivity openings and attribute computed, the filtering is then applied. If ψ^Λ is the filter and Λ is the attribute criteria, then ψ^Λ can be defined as

$$\psi^\Lambda(C) = \begin{cases} C & \text{if } \Lambda(C) \text{ is true} \\ \emptyset & \text{otherwise} \end{cases} \quad (3)$$

The result of the filtering of the image X is then given as:

$$\psi_\Lambda(X) = \bigcup_{x \in X} \psi^\Lambda(\Gamma_x(X)) \quad (4)$$

This represents the union of all connected *foreground* components which meet criterion Λ . The dual counterparts of these operators are attribute closings and thickening respectively and can be defined as

$$\Psi_\Lambda(X) = (\psi_\Lambda(X^c))^c \quad (5)$$

where $X^c = E \setminus X$ denotes the complement of X . This removes connected *background* components which do not meet the criterion Λ . The attribute could be for example area of a connected component which is then compared to Λ which is a predefined threshold and returning true if the value is above the threshold and false otherwise. In our approach we do not require this.

The same principle can be extended to gray scale images (Breen and Jones, 1996; Salembier and Serra, 1995), where connectivity rely on the notion of partitions of flat zones. A partition is defined as the set of non overlapping, non void regions within the image domain E . More formally, Connected operators in this case act on connected components of level set images L_h of image f which can be defined as:

$$L_h(f) = \{x \in E | f(x) = h\}. \quad (6)$$

Where h is the gray level of the image. There is a binarization at every level L_h of the image. For more on connected operators see (Breen and Jones, 1996; Salembier et al., 1998; Urbach et al., 2007), (Kiwanuka and Wilkinson, 2015).

4 DATA COLLECTION

Through a NUFFIC funded project, skin infected images were collected from skin clinics in three Ugandan districts of Kampala, Gulu and Mbarara. First, the patients were clinically examined by dermatologists, then culture laboratory tests were conducted to ascertain and confirm the skin infection. The dermatologists then captured more images using a 4MB pixel resolution phone camera from the patients whose results were indicative of either a viral or bacterial infection. The images were then preprocessed and in some cases were split where it was deemed that different parts of the images were fairly distinct and would aid the classification. 1824 images (912 viral, 912 bacteria) were captured. Fig. 2 shows examples of the sample images for bacterial and viral skin diseases. Each image is of size 80x80 pixels.

5 CONNECTED COMPONENTS FEATURE ENGINEERING

A large number of both size and shape features is available for connected filtering for 2D and 3D imaging modes (Breen and Jones, 1996; Salembier et al., 1998; Urbach et al., 2007; Kiwanuka et al., 2009a). These features enhance the ability of connected filters

to select structures of interest for different imaging modalities. However in this research we utilize them for classification. Specifically, we compute attributes for 2D imaging modes.

5.1 Size based Features

For size based attributes, we considered:

- **Area** - area is easily estimated by counting the number of pixels that constitute a connected component.
- **Perimeter** of a connected component
- **Minimum child gray level** of peak connected component
- **Current gray level** of peak connected component
- **Maximum child gray level** - current gray level

5.2 Shape based Features

Features are considered as shape descriptors provided they satisfy three key properties: translation, scale, and rotation invariance. We considered moment based attributes like moment of inertia, non-compactness, elongation, flatness, sparseness, and jaggedness. For all these attributes and their variants see (Urbach, 2015), (Kiwanuka et al., 2009a), (Kiwanuka et al., 2009b), (Kiwanuka and Wilkinson, 2010), (Quinn et al., 2014), (Kiwanuka and Wilkinson, 2015). Here briefly is a formulation of some of them. The moment-of-inertia $I(C)$ of an object can be defined as its tensor which is equivalent to the covariance matrix multiplied by the number of pixels in a connected component(C). The compactness attribute $N(C)$ is defined as

$$N(C) = \frac{P^2(C)}{4\pi A(C)} \quad (7)$$

where A is the area of each connected component and P is the perimeter. Other moment-invariants can be obtained using geometric interpretation from the eigenvalues of tensor matrix and are derived as follows. Let $e_1(C)$, $e_2(C)$ and $e_3(C)$ be the three (real) eigenvalues of $I(C)$ such that:

$$|e_1(C)| \geq |e_2(C)| \geq |e_3(C)| \quad (8)$$

The measure of *elongation* $\xi(C)$ is given by

$$\xi(C) = \frac{|e_1(C)|}{|e_2(C)|} \quad (9)$$

While *flatness* $F(C)$ is given by:

$$F(C) = \frac{|e_2(C)|}{|e_3(C)|} \quad (10)$$

We also considered four non-normalized central moments and the normalized geometric moments. For more about these features see (Urbach et al., 2007).

In total we computed 14 size and shape features for each connected component.

5.3 Computing Features using the Max Tree Data Structure

We utilized the Max-Tree data structure (Salembier et al., 1998) an efficient data structure for gray scale image processing. In the Max Tree data structure, the filtering process is made of four stages: the creation of Max-Tree, feature computation, filtering, and restitution. In our approach, we only use the first two stages.

Many fast algorithms have been developed to build a Max-Tree like (Salembier et al., 1998; Wilkinson, 2011). Like any other tree based data structure, the Max tree arranges the connected component of an image into a tree with the root node acting as a parent to all subsequent nodes where for the case of gray scale images, a node represents a flat zone L_h where a set of pixels adopts a single gray-level value of the highest node within that subset. Binarization of the image is then carried out at each level h to obtain the thresholded set consisting of peak components, P_h^k , whose gray-level $\geq h$ (k is node index). C_h^k are the components in P_h^k with gray-level h . An example of the Max tree is shown in Fig. 3. There are two ways to compute the attributes. One is during the Max Tree building phase where data needed for computing the node features is collected. This data can then be used to compute the features, that describe shape or size of the peak components represented by the nodes.

Once the features have been computed, then the filtering process is done to decide what connected components preserve usually based on certain rules like the *Direct*, *Min*, *Max*, and *Viterbi* rules (Breen and Jones, 1996), or the *Subtractive* rule (Urbach et al., 2007). However, in our research, rather than filter, we simply stack the features for each image. It is these features that we use as input for training our Gradient boosting model. To deal with the variable number of connected components of the different images, we fix the number of connected components of all images to be equal to the worst case of the number of pixels in the image. In practice, instead of representing the image with pixel values we represent the image as a set of connected components. We then compute the features for those connected components using the Max-Tree data structure. Suppose, the number of connected components in an image is n and the size of the image is $M \times N$, where $n \leq M \times N$ during the

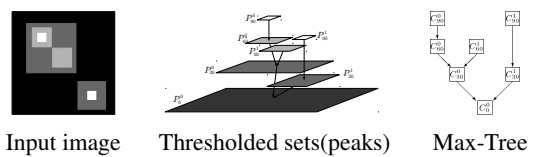


Figure 3: An example of a Max-Tree representation of a simple 4-level image.

feature preparation for training, we enforce that $n = M \times N$ by assigning zeros to the extra components created.

6 CLASSIFICATION

In this section we describe the training process of two approaches:

1. Our approach : connected components feature engineering
2. Convolutional Neural Networks (CNN) approach that trains a model from scratch using our little data that we have. We then use data augmentation and finally use a pre-trained CNN model

6.1 Connected Feature Approach: Implementation

We computed 14 features for each connected component in the image and stacked them. We then normalized each image to have the number of connected components to be equal to the size of the image $M \times N$. The extra connected components have features set at zero. Let n be the actual number of connected component and E the number of pixels in the image. The number of connected components set to zero can be given as the difference $E - n$. During the exploratory analysis we had carried out feature selection to narrow down the features with the most informative for our task.

To establish the performance of our proposed connected attribute filters approach, we ran experiments on the skin disease dataset and evaluated the performance of these features. In all of the experiments, we randomly split the datasets into 80 % and 20% from each class as the training set and the rest as testing set respectively. For the training we used gradient boosting machines classifier. A gradient boosting machine, much like a random forest, is a machine-learning technique based on ensembling weak prediction models, generally decision trees. It uses gradient boosting, a way to improve any machine-learning model by iteratively training new models that specialize in addressing the weak points of the previous mod-

els. The choice of gradient boosting is due to its excellent ability to deal with non perceptual data and being one of the most commonly used techniques in Kaggle competitions besides deep learning.

To ensure that we reduce overfitting, we employed regularization methods that penalize various parts of the algorithm and generally improve the performance of the algorithm. Experimentally:

- Choose a learning rate of 0.05 after experimenting with the rates between 0.05 and 0.2.
- The optimum number of trees for this learning rate was 2435.
- Fixed tree hyperparameters and tune learning rate and assessed speed and performance.
- Tuned tree-specific parameters for decided learning rate.
- Hyperparameter settings was carried and cross validation procedures to get more robust estimates.

6.2 Convolutional Neural Networks (CNN)

We first trained a CNN model from scratch on our dataset but we split the data in 60% training, 20% for validation and 20% testing. For the implementation of CNN, we stacked alternated Conv2D with relu activation and MaxPooling2D layers to augment the capacity of the network and also reduce the size of the feature maps before the flatten layer. We ended with a network with a Dense layer of size 1 using a sigmoid activation. Even with numerous experimentation with various architectures and parameters tuning, it was apparent that the network was overfitting. The training accuracy increased linearly over time, until it reached nearly 78%, whereas the validation accuracy stalled at about 56%. The validation loss reached its minimum after a few epochs and then stalled, whereas the training loss kept decreasing linearly until it reaches near zero.

We then explored data augmentation to deal with the overfitting problem. We trained a new network using data-augmentation configuration. As such, this was not enough to completely get rid of overfitting. To further fight overfitting, we added a Dropout layer to our model before the densely connected classifier. By using regularization and tuning the network's parameters including the number of filters per convolution layer, and the number of layers in the network, we reached an accuracy of 68.6%, a 13% relative improvement.

It became apparent that it would be difficult to go any higher just by training your own CNN from

scratch, because of the not sufficient data to work with. As a next step to improve accuracy on this problem, we explored using a pretrained model.

We used a pretrained network of ImageNet (Krizhevsky et al., 2012) a popular computer vision model trained on a large dataset for large-scale image-classification task with 1.4 million labeled images and 1,000 different classes.

Given that the original dataset is large enough and general enough, then the spatial hierarchy of features learned by the pretrained network can effectively act as a generic model for our skin classification problem even though our problem has completely different classes than those of the original task. A number of skin classification (Bi et al., 2017), (Romero-Lopez et al., 2017), (Pomponiu et al., 2016), studies have used this pretrained CNN models of ImageNet reporting very high accuracy of at least 90%. We used the VGG16 architecture (Simonyan and Zisserman, 2015) because of its simplest and wide use. We considered a pretrained network with feature extraction.

Using the convolutional base of the VGG16 network, trained on ImageNet, to extract features from images, and then train virus and bacteria classifier on top of these features. Due to the skin classes in our dataset, we changed the original 1000 classes classification layer to a binary layer, whose weights are randomly initialized, then added Dense layers on top, and run it end to end. We also employed data augmentation, which as seen earlier improved accuracy earlier and reduced overfitting. Before compiling and training the model, we freeze the convolutional base thus preventing the weights from being updated during training. However this technique is far more computationally expensive.

We were able to achieve an accuracy of about 76.3%. This is much better than that trained from scratch.

6.3 Evaluation

From the experiments, gradient boosting using our features from connected components achieved an accuracy of 75.2% as compared to the best convolution neural networks which achieved 76.3%. The performance of the two approaches is relatively low compared to approaches seen in literature for skin classification like in (Bi et al., 2017), (Romero-Lopez et al., 2017), (Pomponiu et al., 2016), this can be explained by the nature of the dataset. The field conditions, the type of skin and other factors make this dataset difficult to classify. For many images in our dataset as seen in Fig. 2, viral and bacterial patches tend to

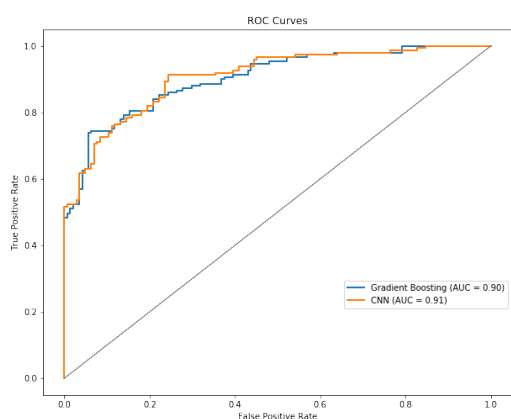


Figure 4: ROC curves for Gradient Boosting and CNN.

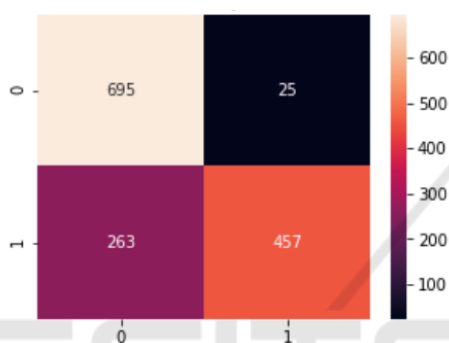


Figure 5: Confusion Matrix with Bacterial (0) and Viral (1) infection.

blend into normal skin, making separating the two classes more difficult as compared to open datasets like those used in (Bi et al., 2017), (Romero-Lopez et al., 2017), (Pomponiu et al., 2016). However, our approach was faster in computing times by at least 56% as seen in Table 1.

The Receiver Operating Characteristic (ROC) curve is shown in Figure 4. ROC curve for our approach and CNN showed a similar performance between the two approaches. The Area Under the Curve (AUC) of 0.90 and 0.91 indicates that the classifier performs well.

The confusion matrix in Fig. 5 shows that the gradient boosting classifier performed well on classifying the bacterial infection (0) as compared to the viral infection (1). This can be attributed to the nature of bacterial infections having a clear morphological visual description of bumps as compared to the viral infections as seen in Fig. 2.

6.4 Computational Timings

Using a standard Core 4 Duo E8400 at 2.0 GHz machine with 16 GB RAM, we performed timings for

Table 1: Performance Evaluation.

Model	Accuracy(%)	Computing Algorithms Time(seconds)
Gradient Boosting using Connected Filters	75.1	216
CNN with augmentation	68.0	313
Pre-trained CNN	76.2	338

the computation of our approach and that of CNN. For the connected attribute filter approach the timings include the time to compute the attributes from the max Tree as well as the training. For the CNN, since the feature engineering is inherently learned during the training, the timing include the whole cycle of, defining the model, compiling the model, and fitting the model. The performance of the two approaches can be seen in Table. 1 where it is clear that our approach was faster in computing times by at least 56%.

7 CONCLUSIONS

In this paper, we proposed an approach for using connected attribute filters for classifying skin infections. With 75.1% level of accuracy, our approach is comparable to the performance of Convolutional Neural Networks. We compared the classification accuracy of a CNN trained from scratch, a pretrained CNN with transfer learning and frozen layers. All three configurations were tested with 364 images and the last-mentioned configuration achieved the highest accuracy of 76.3%. Our approach is at least 56% faster than CNN in computational time. In future, we intend to investigate the performance of our approach when combined with deep learning. This should be possible since connected filters tend to behave by design like deep learning models with the flat zones as hidden layers as used in deep learning, however without back propagation.

REFERENCES

- Barati, E., Sarace, M. M., Mohammadi, A., Adibi, N., and Ahmadzadeh (2011). A survey on utilization of data mining approaches for dermatological (skin) diseases prediction.
- Bi, L., Kim, J., Ahn, E., and Feng, D. (2017). Automatic skin lesion analysis using large-scale dermoscopy images and deep residual networks. *ArXiv*, abs/1703.04197.
- Breen, E. J. and Jones, R. (1996). Attribute openings, thinnings and granulometries. *Comp. Vis. Image Understand.*, 64(3):377–389.
- Heijmans, H. J. A. M. (1999). Connected morphological operators for binary images. *Comp. Vis. Image Understand.*, 73:99–120.
- Karimkhani, C., Dellavalle, R. P., Coffeng, L. E., Flohr, C., Hay, R. J., Langan, S. M., Nsoesie, E. O., Ferrari, A. J., Erskine, H. E., Silverberg, J. I., Vos, T.,

- and Naghavi, M. (2017). Global Skin Disease Morbidity and Mortality: An Update From the Global Burden of Disease Study 2013. *JAMA Dermatology*, 153(5):406–412.
- Kiwanuka, F. N., Ouzounis, G. K., and Wilkinson, M. H. (2009a). Surface-area-based attribute filtering in 3d. In *Proceedings of the 9th ISMM '09*, pages 70–81, Berlin, Heidelberg. Springer-Verlag.
- Kiwanuka, F. N., Ouzounis, G. K., and Wilkinson, M. H. (2009b). Surface-area-based attribute filtering in 3d. In *Proceedings of the 9th ISMM '09*, pages 70–81, Berlin, Heidelberg. Springer-Verlag.
- Kiwanuka, F. N. and Wilkinson, M. (2015). Cluster based vector attribute filtering. In *ISMM*.
- Kiwanuka, F. N. and Wilkinson, M. H. F. (2010). Radial moment invariants for attribute filtering in 3D. In Käthe, U., Montanvert, A., and Soille, P., editors, *Proc. Workshop on Applications of Discrete Geometry and Mathematical Morphology (WADGMM)*, pages 37–41.
- Krizhevsky, A., Sutskever, I., and Hinton, G. E. (2012). Imagenet classification with deep convolutional neural networks. In Pereira, F., Burges, C. J. C., Bottou, L., and Weinberger, K. Q., editors, *Advances in Neural Information Processing Systems 25*, pages 1097–1105. Curran Associates, Inc.
- Liao, H., Li, Y., and Luo, J. (2018). Skin disease classification versus skin lesion characterization: Achieving robust diagnosis using multi-label deep neural networks. *CoRR*, abs/1812.03520.
- Meijster, A. and Wilkinson, M. H. F. (2002). A comparison of algorithms for connected set openings and closings. *IEEE Trans. Pattern Anal. Mach. Intell.*, 24(4):484–494.
- Mennillo, L., Cousty, J., and Najman, L. (2015). A comparison of some morphological filters for improving ocr performance. In Benediktsson, J. A., Chanussot, J., Najman, L., and Talbot, H., editors, *Mathematical Morphology and Its Applications to Signal and Image Processing*, volume 9082 of *Lecture Notes in Computer Science*, pages 134–145. Springer International Publishing.
- Ouzounis, G. K. and Wilkinson, M. H. F. (2011). Hyper-connected attribute filters based on k -flat zones. *IEEE Trans. Pattern Anal. Mach. Intell.*, 33(2):224–239.
- Pomponiu, V., Nejati, H., and Cheung, N. . (2016). Deepmole: Deep neural networks for skin mole lesion classification. In *2016 IEEE International Conference on Image Processing (ICIP)*, pages 2623–2627.
- Quinn, J. A., Munabi, I., and Kiwanuka, F. N. (2014). Automated blood smear analysis for mobile malaria diagnosis. In *In W. Karlen and K. Iniewski, editors, Mobile Point-of-Care Monitors and Diagnostic Devices*. CRC Press 2014.
- Romero-Lopez, A., Burdick, J., i Nieto, X. G., and Marques, O. (2017). Skin lesion classification from dermoscopic images using deep learning.
- Salembier, P. (2015). Study of binary partition tree pruning techniques for polarimetric sar images. In Benediktsson, J. A., Chanussot, J., Najman, L., and Talbot, H., editors, *Mathematical Morphology and Its Applications to Signal and Image Processing*, volume 9082 of *Lecture Notes in Computer Science*, pages 51–62. Springer International Publishing.
- Salembier, P., Oliveras, A., and Garrido, L. (1998). Anti-extensive connected operators for image and sequence processing. *IEEE Trans. Image Proc.*, 7:555–570.
- Salembier, P. and Serra, J. (1995). Flat zones filtering, connected operators, and filters by reconstruction. *IEEE Transactions on Image Processing*, 4:1153–1160.
- Salembier, P. and Wilkinson, M. H. F. (2009). Connected operators: A review of region-based morphological image processing techniques. *IEEE Signal Processing Magazine*, 26(6):136–157.
- Serra, J. (1998). Connectivity on complete lattices. *J. Math. Imag. Vis.*, 9(3):231–251.
- Simonyan, K. and Zisserman, A. (2015). Very deep convolutional networks for large-scale image recognition. In *International Conference on Learning Representations*.
- Soille, P. (2008). Constrained connectivity and connected filters. *IEEE Trans. Pattern Anal. Mach. Intell.*, 30(7):1132–1145.
- Sun, X., Yang, J., Sun, M., and Wang, K. (2016). A benchmark for automatic visual classification of clinical skin disease images. In *ECCV*.
- Urbach, E. (2015). Intelligent object detection using trees. In Benediktsson, J. A., Chanussot, J., Najman, L., and Talbot, H., editors, *Mathematical Morphology and Its Applications to Signal and Image Processing*, volume 9082 of *Lecture Notes in Computer Science*, pages 289–300. Springer International Publishing.
- Urbach, E. R., Roerdink, J. B. T. M., and Wilkinson, M. H. F. (2007). Connected shape-size pattern spectra for rotation and scale-invariant classification of grayscale images. *IEEE Trans. Pattern Anal. Mach. Intell.*, 29:272–285.
- van de Gronde, J. and Roerdink, J. (2014). Group-invariant colour morphology based on frames. *Image Processing, IEEE Transactions on*, 23(3):1276–1288.
- Westenberg, M. A., Roerdink, J. B. T. M., and Wilkinson, M. H. F. (2007). Volumetric attribute filtering and interactive visualization using the max-tree representation. *IEEE Trans. Image Proc.*, 16:2943–2952.
- Wilkinson, M. H. F. (2011). A fast component-tree algorithm for high dynamic-range images and second generation connectivity. In *Proc. Int. Conf. Image Proc. 2011*, pages 1041–1044.